

N 9 4 - 1 7 3 5 5

MEASUREMENTS OF MICROLENS PERFORMANCE

D. Shough, B. Herman, and G. Gal
Lockheed Palo Alto Research Laboratory
3251 Hanover Street, Palo Alto, California 94304

ABSTRACT

We present results of laboratory evaluations of several microlens types that have been designed and fabricated at the Lockheed Research and Development Division. The microlenses include wideband and dispersive types, in isolation and in arrays, and fabricated with binary or grayscale methods. Different lens pixel geometries are considered, including square, hexagonal, and skewed microlenses. We describe our micro-optics laboratory testbed which has been designed for the evaluation of individual lenslets or 2D arrays at selected spectral wavelengths. Measurement capabilities include focal length, point-spread functions, wavefront quality, and modulation transfer functions. Our present effort focuses on the results of point spread function measurements and their comparison with design predictions.

1.0 INTRODUCTION

The Lockheed Research & Development Division (R&DD) has an ongoing effort in the research and development of micro-optics technology. The effort encompasses research and development of innovative micro-optics elements for systems applications that require the design, fabrication, and optical performance evaluation of microlenses and microlens arrays. The purpose of this paper is to report the establishment of a micro-optics metrology laboratory and to describe some of the techniques and equipment that have been developed specifically for the study of microlenses, both as individual elements and as arrays.

Testing microlenses is in principle no different than testing any other optical element. The same parameters need to be measured and the techniques required are the familiar methods utilized in any conventional optical testbed. However, in many cases the measurement of microlenses presents practical problems because of the size of the elements. Microlenses of interest to us have diameters between 50 μm and a few millimeters and have speeds between $f/1$ and $f/10$.

On an individual basis as well as for arrays, measurements that are of interest are: the focal length; point-spread function (PSF); wavefront quality; modulation transfer function (MTF); micro-

lens surface quality, shape, and radius; transmission efficiencies; and wavefront properties. For testing a microlens array, we must include dropouts and uniformity across the array. This is especially important for integrated devices such as focal plane arrays.

Internally cooled apertures and agile beam steering (ABS) units¹ require the utilization of a special grouping of array lenses to produce combined pairs defined by Gabor as superlenses.² These lenslet arrays have interesting optical properties and it is necessary to measure their MTF and subsequent image formation properties. Detailed optical performance evaluation is our long-term objective.

2.0 MICRO-OPTICS TESTBED

We have established a laboratory dedicated to testing micro-optics. Table 1 outlines our test capabilities for single microlenses and/or microlens arrays.

Testing an individual microlens allows detailed measurements of its properties. This is very important in order to verify the design and fabrication of microlenses. The side lobes of the PSF, which might cause cross-talk in adjacent pixels of a focal plane array, can be measured, or the ripple in the wavefront quality, which might cause severe image degradation can be examined. The main problems are providing enough power through the small size of a single microlens and magnifying the image to a reasonable size.

For some applications, such as integrated focal planes, each lens in the array must be tested to ensure that manufacturing problems did not cause one or more microlenses to drop out or to be substandard. Testing every microlens in a 100 by 100 array requires 1 week if each lens takes only 1 min. This precludes the detailed testing that we do for individual microlenses.

These optical measurements may be performed according to a test plan at a variety of wavelengths from various sources:

- CO₂ laser at 10.6 μm
- Lead-salt lasers at 8, 10, 12, and 14 μm . Other lead-salt lasers from 3.3 to 20 μm can easily be added
- Blackbody source with monochromator adjustable from 0.4 μm to 20 μm
- HeNe laser at 3.39 μm
- HeNe laser at 1.52 μm
- Solid state lasers from 0.7 to 1.6 μm

3.0 POINT-SPREAD FUNCTION (PSF) MEASUREMENT

The PSF is the image of a point source formed by a lens. Measurement of the PSF provides a detailed examination of the performance of a fabricated lens. The basis for our measurements of

1. Gal, G., et al. "Micro-Optics Technology and Sensor System Applications," Conference on Binary Optics, Huntsville, AL, 1993.
2. Hutley, M. C., and R. F. Stevens, "The Formation of Integral Images by Afocal Pairs of Lens Arrays ("Superlenses")," *Microlens Arrays*, M. C. Hutley, Ed., IOP Short Meeting Series No. 30, Institute of Physics, Vol. 199, IOP Publishing, Ltd., UK.

the PSF (Figure 1) is to place the microlens array on a computer-controlled XYZ translation stage and to examine the intensity from individual microlenses. The PSF is magnified by a microscope objective onto a detector. The system is flexible, accurate, and extendible.

3.1 CO₂ LASER SOURCE

All measurements presented in this paper use a 10 W CO₂ laser operating at 10.6 μm . A rotating polarization attenuator prevents thermal damage to the optics. A quartz window acts as a dichroic beam splitter, allowing us to coalign a visible HeNe laser for alignment purposes. The laser beam passes through a mechanical chopper and two apertures before striking the lens array. The illuminated area of the array is a 0.5-in.-diameter circle.

The CO₂ laser produces a nearly collimated beam and has more than enough power for the desired measurements. Because of the small size of the microlenses, the collimation requirements for the incident beam are very lax. To have less than one-quarter wave peak-to-peak error across a microlens, the radius of the wavefront should be greater than 5 mm, i.e., the wavefront appears collimated if the beam focus is at least 5 mm away from the microlens. Even then the effect of using a slightly diverging beam is to test the microlenses at an incorrect magnification.

3.2 LEAD-SALT LASERS

For testing dispersive microlenses³ (which simultaneously focus and disperse light in a wavelength band), it is necessary to vary the spectral wavelength. We are in the process of adding four lead-salt lasers that operate at 8, 10, 12, and 14 μm to our set-up. All four lasers are mounted within one LN₂ dewar. To switch between lasers, we are installing a kinematic base that allows easy and repeatable repositioning of the dewar in four different positions corresponding to the lasers. We switch between the CO₂ and the lead-salt lasers by removing a mirror mounted on another kinematic base.

The lead-salt lasers emit approximately 1 mW of power from an area of 10 by 20 μm . This produces a beam with a large divergence and low power through the microlenses. Therefore, we must collimate the beam in order to increase the amount of power through the microlenses.

When switching between lasers, we do not expect perfect alignment of the sources, which will cause an apparent shift in the position of the PSF. We calibrate for this effect by first testing a microlens that does not have any dispersion (and, hence, does not deflect the focused spot).

3.3 MAGNIFICATION OF THE PSF

The output of the microlenses is collected by an Ealing all-reflecting microscope objective. The numerical aperture of the 36X objective is 0.50. It has a central obscuration of 12.5%, a field of view of 500 μm , and a focal length of 5.2 mm. The working distance for an unmodified objective is 8.0 mm. The light baffles in an unmodified Ealing objective (Figure 2) proved to be unusable for our purposes because the baffles let light pass straight through the objective to the image plane. We added a new stop to eliminate this effect. The exact size and position for the new stop was determined by trial and error.

The resolution of an ideal microscope objective with no central obstruction and with a numerical aperture of 0.5 is 26 μm . The effect of the obstruction on the PSF is to decrease the total power and to increase the power outside the central lobe. The radial distribution of power becomes

3. Herman, B., and G. Gal, "Theory of Dispersive Microlenses," Conference on Binary Optics, Huntsville, AL, 1993.

$$I(r) = \pi P_1 \left(\frac{D}{2\lambda f} \right)^2 \left| \frac{2J_1\left(\frac{\pi D r}{\lambda f}\right)}{\left(\frac{\pi D r}{\lambda f}\right)} - \frac{d^2}{D^2} \frac{2J_1\left(\frac{\pi d r}{\lambda f}\right)}{\left(\frac{\pi d r}{\lambda f}\right)} \right|^2$$

which is basically the difference between Airy patterns caused by the unobstructed objective and the obscuration. The last term is the contribution of the obscuration. The shape change is shown in Figure 3, with the obscured objective shown in black and the equivalent, unobscured objective shown in gray. The measured PSF out of the detector is the convolution of the PSF of the microlens, the PSF of the microscope objective, and the response of the detector.

In our current setup, the distance from the objective to the detector is 82 cm. Adding 4 cm for the separation of the principal plane and the objective shoulder gives an image distance of 86 cm. This produces a magnification of 160 for the 36X objective.

3.4 DETECTION

All data presented in this paper were taken using a HgCdTe detector cooled in a LN₂ dewar. The detector area is 1 mm by 1 mm. The microscope objective is used at 160X magnification; this corresponds to 6.25 μm at the plane of the PSF.

The light source is mechanically chopped at 1 kHz. The output of the detector is fed through a preamplifier specifically matched to the detector. The preamplifier output is fed to a lock-in amplifier which is read by the computer.

The range of the detector/preamplifier/lock-in amplifier extends from 3.3 pW to 0.4 μW, a dynamic range of over 5 decades. This allows detailed examination of the light outside the central diffraction lobe. The disadvantage to this setup is the long time required to complete a scan. A 101 by 101 2D scan or a 21 by 21 by 21 3D scan using a time delay of 1 s between readings requires 3 h.

Some scans require overnight runs with the result that the detector's LN₂ dewar warms up. This causes loss of all data until the dewar is refilled. Similarly, the power output of the CO₂ laser drifts over a range of 25 to 1. We are adding a second detector whose purpose is to monitor the output power. Future data will include corrections for these power fluctuations.

3.5 PSF, CONVOLUTION, AND SCANNING

The microlenses we have tested produce PSFs with diameters of 33 μm. This is magnified 160 times by the microscope objective and imaged onto the plane of the detector. At the detector, the magnified PSF diameter is 5.3 mm. The detector integrates the intensity over its 1 mm by 1 mm surface area to measure the power level.

To measure the spatial distribution of the PSF of the microlens, either the detector and microscope objective or the microlens must be moved. Either motion is approximately equivalent and moving just the microlens is far easier. The microlens array is mounted on a set of computer controlled Klinger XYZ translation stages with a resolution of 0.1 μm over a range of 50 mm. Maximum speed is 400 μm/s.

The measured value out of the detector is the convolution of the PSF of the microlenses, the PSF of the microscope objective, and the area or PSF of the detector divided by system magnification (160).

$$\begin{aligned}
 p(x, y) &= l(x, y) \otimes \otimes m(x, y) \otimes \otimes d\left(\frac{x}{m}, \frac{y}{m}\right) \\
 &= l(x, y) \otimes \otimes s(x, y)
 \end{aligned}$$

where l , m , and d are the PSFs from the micro-optic lens, the microscope objective, and the detector, respectively, and $\otimes \otimes$ is a two-dimensional convolution. We are trying to measure l , the spatial distribution of the microlens PSF. This can be done by decorrelating l from the system response s .⁴ In the Fourier transform frequency domain,

$$L(\xi, \eta) = \frac{S(\xi, \eta)P^*(\xi, \eta)}{|S(\xi, \eta)|^2 + \gamma|P(\xi, \eta)|^2}$$

where capitol letters indicate the Fourier transform, γ is the Lagrangian multiplier, and P is a smoothing function. The software exists but has not yet been applied to this problem.

3.6 TESTING PROCEDURES

After placing a microlens array on the XYZ translation stages, a quick coarse scan is made to determine the approximate coordinates of the microlens positions. The image is compared to the expected pattern of microlenses. Next, 2D and 3D scans are made in the vicinity of a single lens in order to refine the XYZ coordinates for the best focus. The position of best focus can be measured to within 2 μm . A final high-resolution scan is made in the plane of best focus.

A software package has been assembled for controlling the experiment and collecting the data. A variety of routines were programmed to allow control of the translation stages, reading of the lock-in-amplifier, and storing the data. These routines were then included within a program to perform 1D, 2D, and 3D scans of the PSF. The number of steps in each direction, the step size, the starting and ending positions, the dwell times at the start of each scan line, and the time constant for the lock-in-amplifier are all adjustable. To take advantage of the wide dynamic range of the detector, the computer program checks the voltage read against the previously set lock-in-amplifier sensitivity, changes scale as needed, and waits for the new reading.

The measured PSF is visualized using commercial software for the analysis of scientific data and custom software for the display of 3D shaded surfaces.

4.0 RESULTS

We now present measured PSF from four different multilevel Fresnel microlenses as indicated in Table 2. Each microlens was designed to concentrate light onto a detector on the back surface of the substrate. The focal lengths indicated are within the material and are the same as the thicknesses of the substrates.

Each microlens is presented with results from a 100- by 100- μm scan with a scan step size of 1 μm . The predicted PSF at the same scale is shown for comparison. No attempt was made to deconvolve the microlens PSF with that of the microscope objective or the detector.

4. Gal, G., and W. G. Opyd, "Determination of the Detector Spatial Responsivity by Signal Decorrelation in Spot Scan Measurements," *IEEE 1982 Conference Record of the 16th ASILOMAR Conference on Circuits, Systems, and Computers*, pp. 62-66.

4.1 WIDEBAND SQUARE Si

The square microlens on silicon substrate data represent one of the first microlenses we fabricated. The total thickness of the Fresnel element is given as $\bar{\lambda}/(n - 1)$, where $\bar{\lambda}$ is the design wavelength and n is the index of refraction. Unfortunately, an error was made in the fabrication of the silicon microlenses which were etched to a depth of $\bar{\lambda}/n$. The correct depth is $4.2 \mu\text{m}$ while the actual depth was $3.1 \mu\text{m}$. The effect of this was to change the design wavelength from $10.5 \mu\text{m}$ to $7.4 \mu\text{m}$. This introduced a chromatic error when testing the lens at $10.6 \mu\text{m}$ due to the Fresnel nature of the element. (The consequence was that energy increased in the side lobes of the PSF.) The reason we show these results is to show our capability to measure the effects of fabrication errors. Consequently, the energy increases in the side lobes of the PSF.

The measured and predicted PSFs for the incorrectly etched lens are shown in Figure 4. The effects of the incorrect etching depth are readily apparent in the four extra side lobes.

4.2 WIDEBAND SQUARE CdTe

The wideband, square CdTe microlenses were correctly fabricated. They are binary, 3-mask (8-level) Fresnel lenses designed for operation at $10.5 \mu\text{m}$ and tested at $10.6 \mu\text{m}$. The width of the central peak in the PSF is $33 \mu\text{m}$.

Figure 5 shows a coarse scan covering an area of 250 by $250 \mu\text{m}$ with a scan step size of $5 \mu\text{m}$. The lens array was rotated with respect to the scan axis. The peak intensities are 23 times the mean. The portion of the array shown contains densely packed microlenses. Clearly shown are the repeatability of the microlenses and the concentration of the light into a small area. When fabricated into an integrated focal plane, a 100% effective fill factor can be obtained while allowing room on the back substrate surface for circuitry.

Figure 6 shows a fine scan of a CdTe lens with the scan covering 100 by $100 \mu\text{m}$ and a scan step size of $1 \mu\text{m}$. Predicted and measured performances are shown in Figures 6a and 6b. Figure 6c shows the measured data rendered as a three-dimensional surface.

4.3 WIDEBAND HEXAGONAL CdTe

Figure 7 shows results from a test array that contains both dispersive and non-dispersive microlenses with square, skewed square, and hexagonal shapes. The portion shown contains on-axis hexagonal lenses and first-order dispersive skewed lenses. Some portions of the array are densely packed while some areas are sparsely packed. The sparse areas allow testing away from the peak of the PSF without interference from neighboring lenses. Figure 7 shows the results of a coarse scan used to determine the lens locations. The scan is 10 by 0.5 mm with a scan step size of $20 \mu\text{m}$.

Figure 8 shows detailed scans from a single microlens. The scan area is 100 by $100 \mu\text{m}$ with scan steps of $1 \mu\text{m}$. The data are from an on-axis, nondispersive hexagonal lens.

4.4 DISPERSIVE SKEWED CdTe

Figure 9 shows the expected multispectral output of the skewed dispersive microlens. Separate images are shown for 8 , 10 , 12 , and $14 \mu\text{m}$. We expect to be testing testing at these wavelengths shortly.

Figure 10 shows detailed scans of single skewed square first-order dispersive microlenses. As can be seen, the shape is distorted from the predicted PSF.

The asymmetric shape of the PSF in Figure 10 is due to the limited acceptance angle of the microscope objective. Figure 11 shows the intersection of the acceptance angle of the 0.5 NA microscope objective with the off-axis cone of light out of a dispersive microlens. The overlap is a thin sliver that causes the severe diffraction effects seen. In an integrated focal plane, this is not a problem because the detector is integrated into the back side of the substrate. Two methods for overcoming this test problem are (1) tilt the microscope objective and (2) micro etch the substrate surface to redirect the output.

5.0 FABRICATION PROCESS CONTROL

5.1 WAVEFRONT QUALITY TESTING

We expect to be creating microlens arrays for use in an ABS unit operating at $1.53 \mu\text{m}$. Initial tests will be similar to our current procedure for measuring the PSF from individual microlenses, with the exception of using near-IR sources, optics and detectors. This should be easy compared to working at $10.6 \mu\text{m}$.

When a complete ABS unit is available, we will place it in a Michelson interferometer to test its wavefront quality. The interferometer is aligned with a large ($> 100 \lambda$) amount of tilt between the reference and test beams. This allows analysis of the interferograms using spatial phase shifting interferometry (SPSI). The Optical Metrology Group at Lockheed R&DD has extensive experience using SPSI to obtain high resolution (640 by 480 pixel) and high accuracy ($\lambda/20$ rms per pixel) wavefront maps from various optical systems. This has included transient effects due to shock waves, scan mirror distortion, and testing near IR windows for process-induced aberrations.⁵

The interferometer requires modification to allow easy testing at various scan angles. The modification will consist of placing the mirror in the arm of the interferometer that contains the ABS unit on a lever attached to a rotating stage. As the beam is steered, the mirror rotates to reflect the beam back through the ABS unit.

5.2 TESTING LARGE ARRAYS

For some applications, such as integrated focal planes, each lens in the array must be tested to ensure that manufacturing problems do not cause one or more microlenses to be substandard. Our current apparatus could, in principle, be used to test every lens in a 100 by 100 array of microlens. A moderate resolution (101 by 101 pixels) scan requires around 3 h—the entire array would be tested in 3.5 years! To test the entire array in 1 week, only 1 min per lens is allowed. This amount of time would allow only a very coarse scan.

The testbed is being enhanced with the addition of a pyroelectric vidicon camera to speed up the acquisition of the PSF data. An image is grabbed in 1/30 of a second. We still have the XYZ translation stages to allow us to move from lens to lens. The down side to using the camera is that the dynamic range and signal-to-noise ratio are much worse than our current setup. This makes the camera unsuited to measuring the side lobes in the PSF.

5. Shough, D. M., O. Y. Kwon, and D. F. Leary, "Spatial Phase-Shifting Interferometry for Measurement of Aero-Optical Effects," 1992 AIAA Annual Interceptor Conference, Huntsville, AL.

The detector area is a 17-mm-diameter circle with a resolution of 270 TV lines. The diameter corresponds to a circle with a diameter of 106 μm in the plane of the PSF. The damage level is 1 mW/cm^2 at the detector face plate. This corresponds to a point source with a total power of 37 μW being reimaged by our 160X magnification objective. This, in turn, corresponds to an irradiance of 3.7 mW/mm^2 through a 100- μm square lens. The total power through our 0.5-in. aperture should be less than 465 mW. This is a concern with the CO_2 laser but not with the 1 mW lead-salt lasers, unless the entire energy is collected into a beam with a diameter of less than 0.65 mm.

6.0 SUMMARY

The Micro-Optics Technology Group within Lockheed R&DD has designed and fabricated individual microlenses and arrays of microlenses that we have experimentally evaluated. The measurement of properties of microlenses and microlens arrays presents some new challenges. We have listed some of the critical parameters and main features of microlenses that need to be measured in order to characterize their optical performance. The measurement of properties of individual microlenses required some originality and modifications of existing optical testbeds and measurement methods.

We have described our current laboratory testbed and shown results of monochromatic PSF measurements for a variety of fabricated microlenses. This year we will expand our capabilities to include testing at various IR wavelengths for dispersive microlenses. Our future plans are to provide testing for large microlens arrays and to do interferometric testing of micro-optic windows.

TABLE I. MICRO-OPTICS TESTBED CAPABILITIES MATRIX

Capabilities	Single Microlenses	Arrays	Systems
PSF	✓	✓	✓
Wavefront	✓		✓
Shape	✓	✓	

TABLE 2. RESULTS ARE PRESENTED FOR FOUR DIFFERENT MULTILEVEL FRESNEL MICROLENSES WITH THE INDICATED PROPERTIES

Type	Shape	Material	Width (μm)	Focal Length (μm)	Design Wavelength (μm)
Wideband	Square	Si	100	525	7.4
Wideband	Square	CdTe	100	417	10.5
Wideband	Hexagonal	CdTe	115	417	10.0
Dispersive	Skewed	CdTe	100	417	10.0

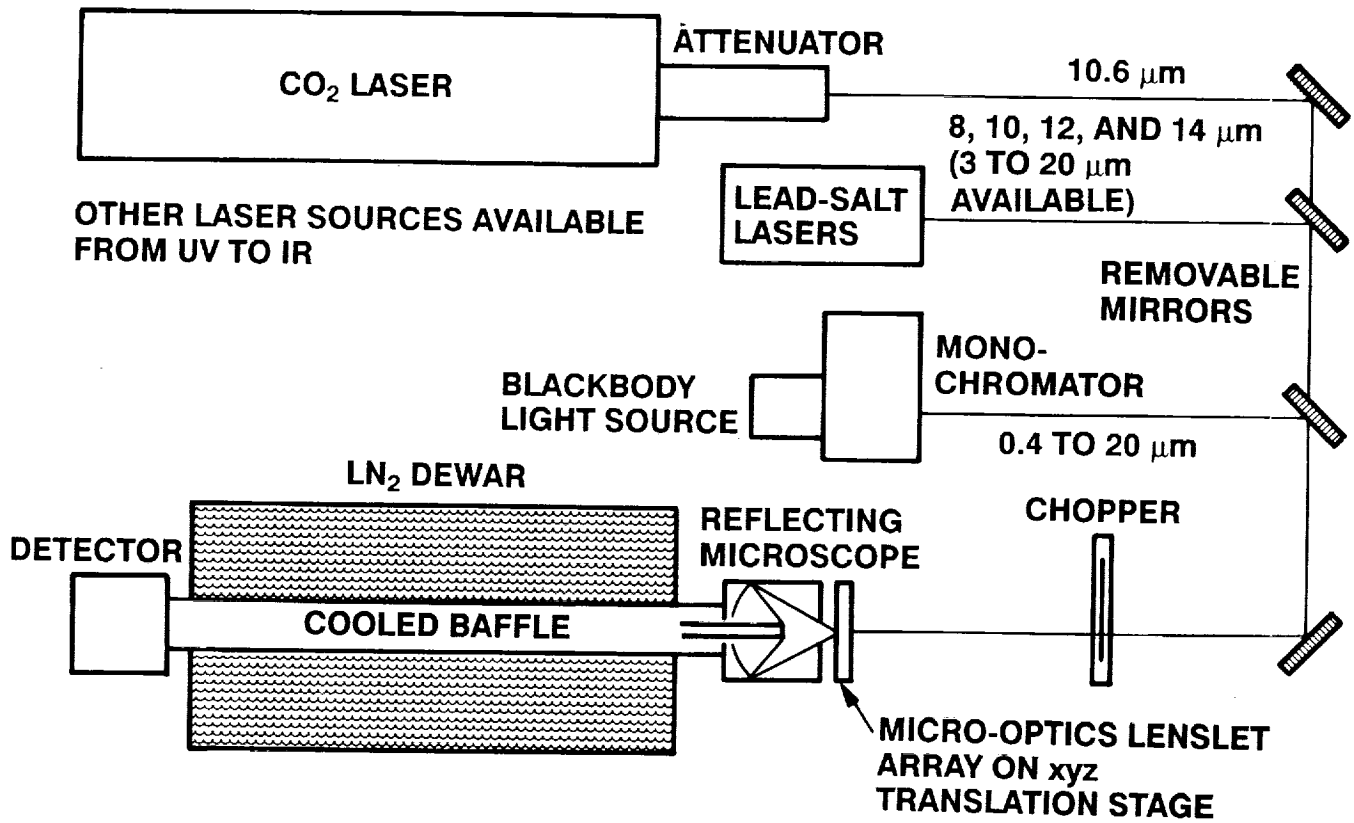


FIGURE 1. CONCEPTUAL DRAWING SHOWING KEY COMPONENTS FOR MEASUREMENT OF PSF.

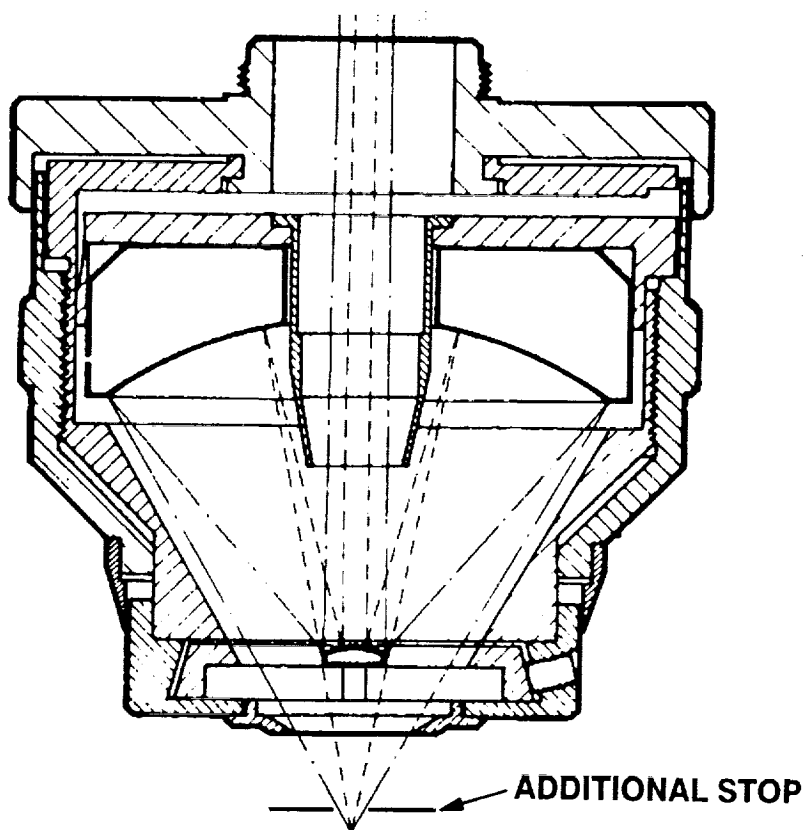


FIGURE 2. COOLING MICROSCOPE OBJECTIVE WITH ADDITIONAL STOP.

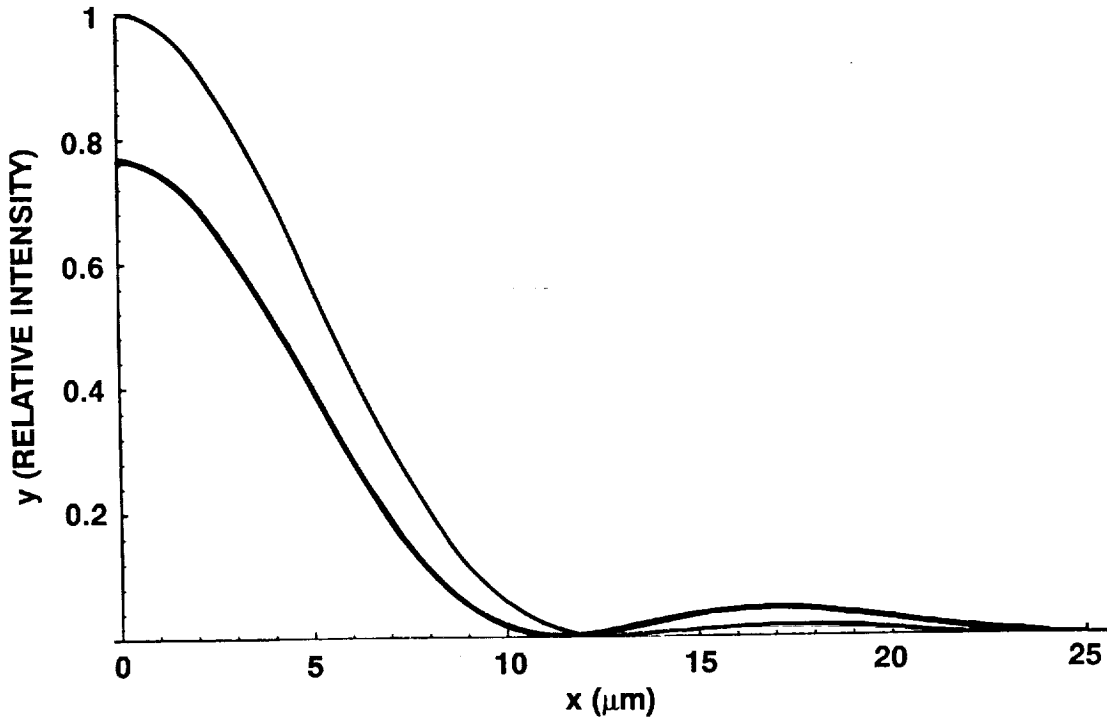


FIGURE 3. PSF WITH (BLACK) AND WITHOUT (GRAY) CENTRAL OBSCURATION.

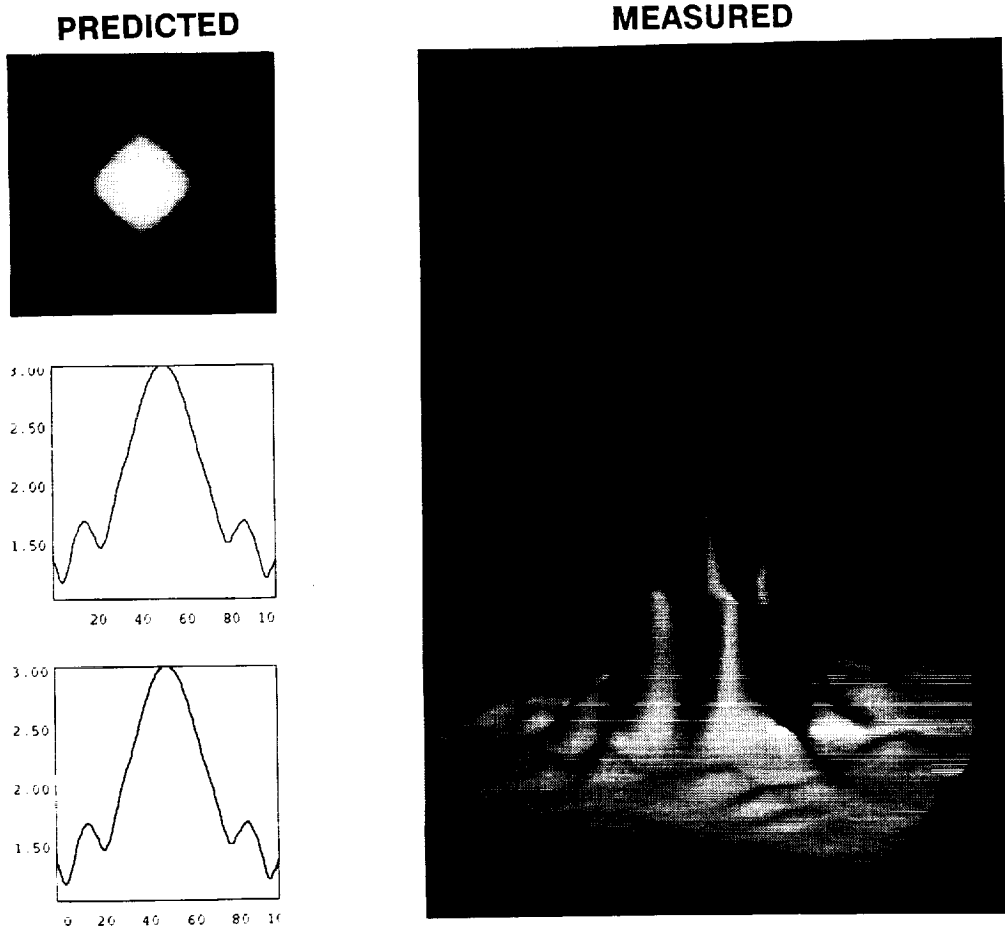


FIGURE 4. PREDICTED AND MEASURED PSFs FOR WIDEBAND, SQUARE, Si MICROLENS.

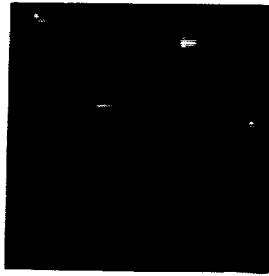


FIGURE 5. COARSE SCAN SHOWS PSFs FROM ARRAY OF MICROLENSSES.

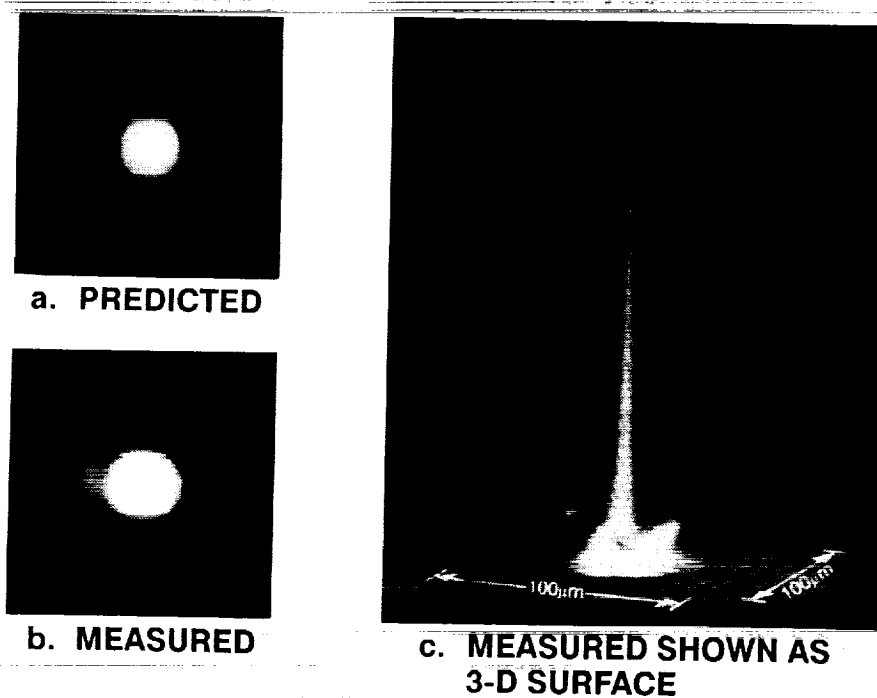


FIGURE 6. PREDICTED AND MEASURED PERFORMANCE OF SQUARE CdTe MICROLENS.

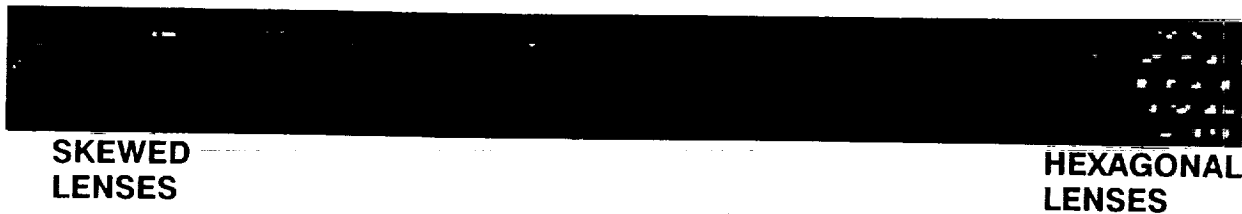


FIGURE 7. COARSE SCAN OF CdTe TEST ARRAY.

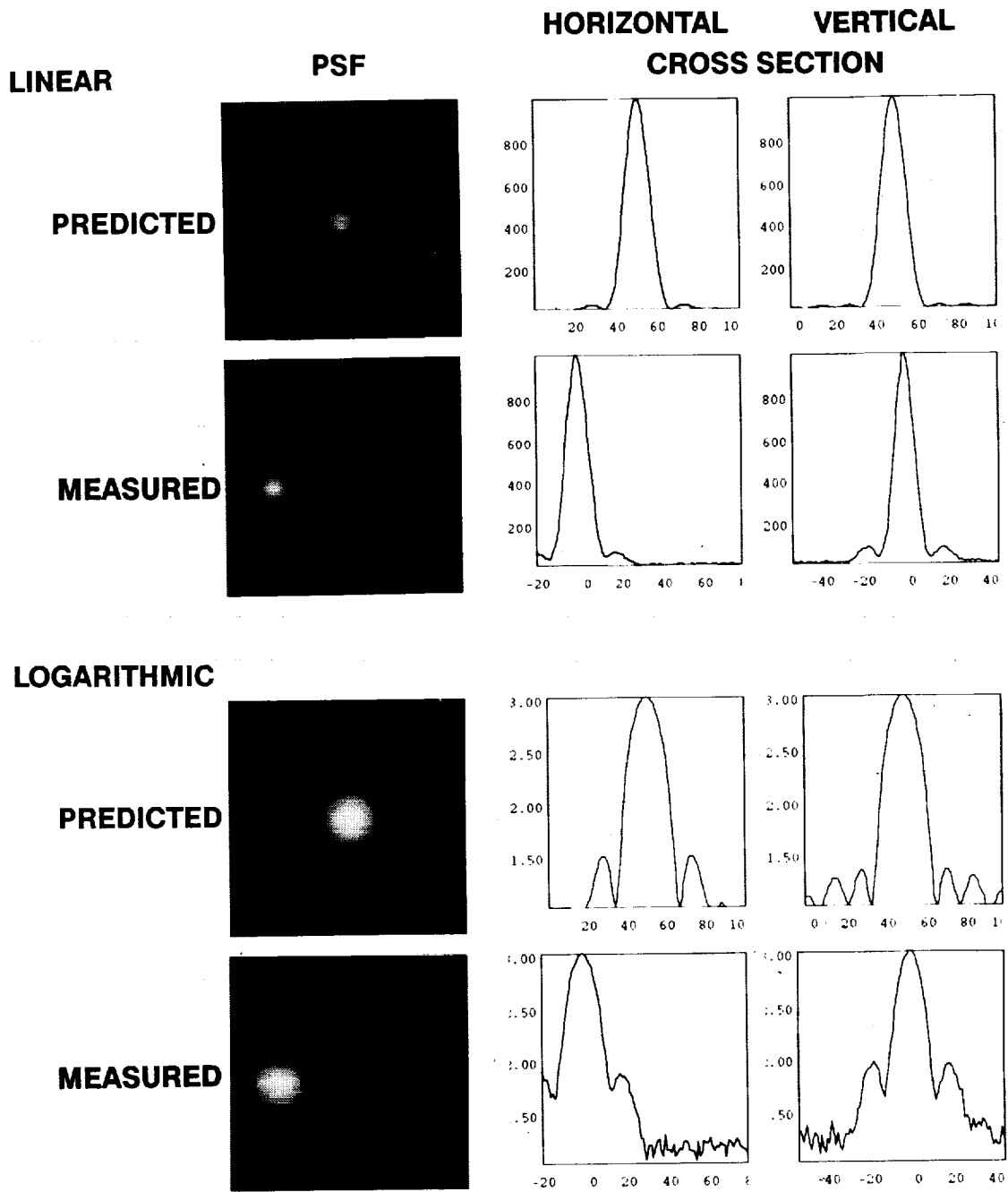


FIGURE 8. DETAILED SCAN OF WIDEBAND HEXAGONAL MICROLENS.

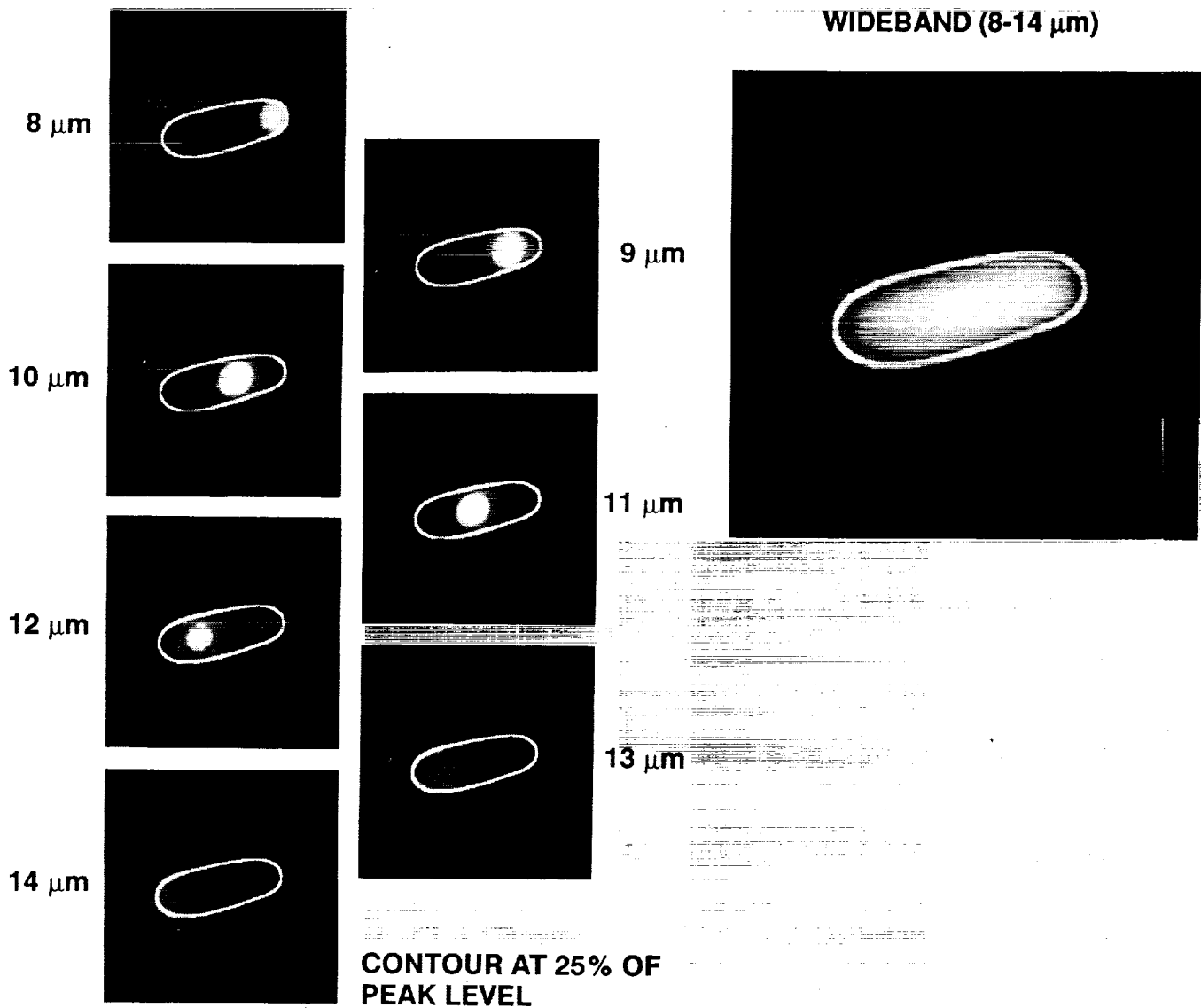


FIGURE 9. PREDICTED MULTISPECTRAL RESPONSE OF SKEWED DISPERSIVE MICROLENS.

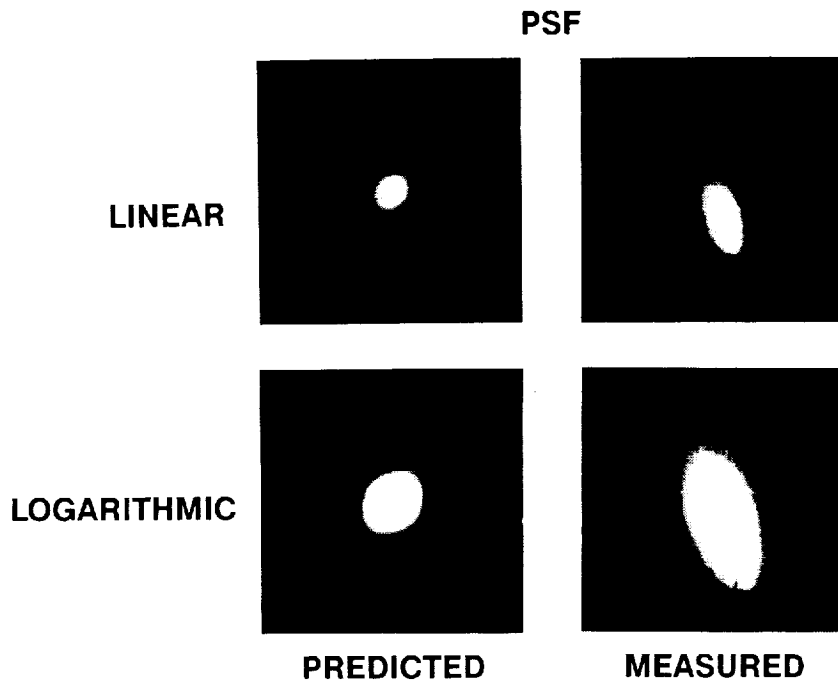


FIGURE 10. DETAILED SCAN OF SKEWED DISPERSIVE CdTe MICROLENS.

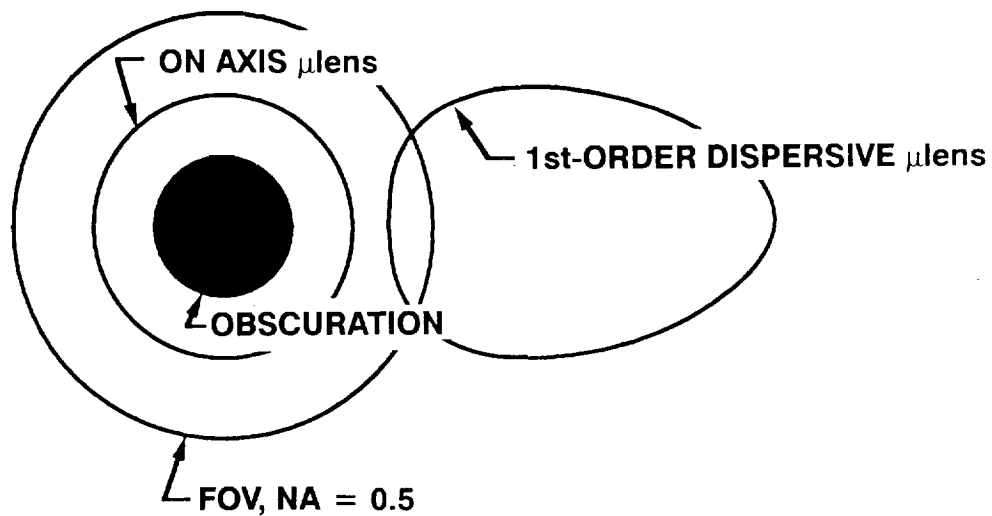


FIGURE 11. OFF-AXIS BEHAVIOR OF MICROSCOPE OBJECTIVE.

1. The first part of the document discusses the importance of maintaining accurate records of all transactions. It emphasizes that this is crucial for ensuring the integrity of the financial data and for facilitating audits.

2. The second part of the document outlines the various methods used to collect and analyze data. It includes a detailed description of the sampling techniques employed and the statistical tests used to evaluate the results.

3. The third part of the document provides a comprehensive overview of the findings of the study. It highlights the key trends and patterns observed in the data and discusses their potential implications for the industry.

4. The fourth part of the document concludes the study by summarizing the main points and offering recommendations for future research. It suggests that further investigation is needed to explore the underlying causes of the observed trends.

5. The fifth part of the document contains a list of references to the sources used in the study. This includes academic journals, books, and other relevant publications that provide a theoretical foundation for the research.

6. The sixth part of the document includes a list of appendices that provide additional information and data. These appendices are intended to support the main text and provide a more complete picture of the study's findings.

7. The seventh part of the document contains a list of figures and tables that illustrate the data presented in the study. These visual aids are designed to make the information more accessible and easier to understand.

8. The eighth part of the document includes a list of footnotes that provide additional details and clarifications. These footnotes are used to address specific points raised in the main text and to provide a more thorough explanation of the research methodology.

9. The ninth part of the document contains a list of acknowledgments that recognize the contributions of individuals and organizations that supported the study. This section is a way to express gratitude and acknowledge the help of others.

10. The tenth part of the document includes a list of contact information for the authors and the research institution. This information is provided so that interested parties can reach out for more information or to request copies of the study.

11. The eleventh part of the document contains a list of definitions for key terms used in the study. This section is intended to ensure that all readers have a clear understanding of the terminology used throughout the document.

12. The twelfth part of the document includes a list of abbreviations and acronyms used in the study. This section is designed to make the document more concise and easier to read by using shorter forms for commonly used terms.

13. The thirteenth part of the document contains a list of references to the sources used in the study. This section is a key component of the document as it provides a way to verify the information and to explore the research further.

14. The fourteenth part of the document includes a list of appendices that provide additional information and data. These appendices are intended to support the main text and provide a more complete picture of the study's findings.

15. The fifteenth part of the document contains a list of figures and tables that illustrate the data presented in the study. These visual aids are designed to make the information more accessible and easier to understand.

16. The sixteenth part of the document includes a list of footnotes that provide additional details and clarifications. These footnotes are used to address specific points raised in the main text and to provide a more thorough explanation of the research methodology.

17. The seventeenth part of the document contains a list of acknowledgments that recognize the contributions of individuals and organizations that supported the study. This section is a way to express gratitude and acknowledge the help of others.

18. The eighteenth part of the document includes a list of contact information for the authors and the research institution. This information is provided so that interested parties can reach out for more information or to request copies of the study.

19. The nineteenth part of the document contains a list of definitions for key terms used in the study. This section is intended to ensure that all readers have a clear understanding of the terminology used throughout the document.

20. The twentieth part of the document includes a list of abbreviations and acronyms used in the study. This section is designed to make the document more concise and easier to read by using shorter forms for commonly used terms.